ACS Biomaterials SCIENCE & ENGINEERING
Article
Cite This: ACS Biomater. Sci. Eng. 2019, 5, 6361−6373
pubs.acs.org/journal/abseba

Formic Acid Regenerated Mori, Tussah, Eri, Thai, and Muga Silk Materials: Mechanism of Self-Assembly

Ye Xue,[†,‡,⊥] Fang Wang,[∥,⊥] Maria Torculas,[†] Samuel Lofland,[†] and Xiao Hu*[,†,‡,§]

[†]Department of Physics and Astronomy, [‡]Department of Biomedical Engineering, and [§]Department of Molecular and Cellular Biosciences, Rowan University, Glassboro, New Jersey 08028, United States

[∥]Center of Analysis and Testing, Nanjing Normal University, Nanjing 210023, China

Supporting Information

ABSTRACT: Flexible and water-insoluble regenerated silk materials have caught considerable interest due to their mechanical properties and numerous potential applications in medical fields. In this study, regenerated Mori (China), Thai, Eri, Muga, and Tussah silk films were prepared by a formic acid-calcium chloride (FA) method, and their structures, morphologies, and other physical properties were comparatively studied through Fourier transform infrared spectroscopy (FTIR), wide-angle X-ray scattering (WAXS), scanning electron microscopy (SEM), differential scanning calorimetry (DSC), dynamic mechanical analysis (DMA), and thermogravimetric analysis (TGA). FTIR results demonstrated that the secondary structures of those five types of silk films are different from those of their respective natural silk fibers, whose structures are dominated by stacked rigid intermolecular β-sheet crystals. Instead, intramolecular β-sheet structures were found to dominate these silk films made by FA method, as confirmed by WAXS. We propose that silk I-like structures with intramolecular β-sheets lead to water insolubility and mechanical flexibility. This comparative study offers a new pathway to understanding the tunable properties of silk-based biomaterials.

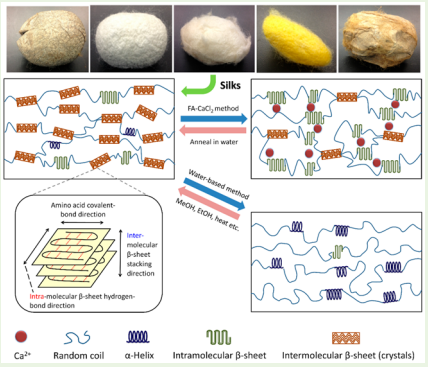

KEYWORDS: *intermolecular and intramolecular β-sheet, silk, self-assembly mechanism, insolubility, flexibility*

1. INTRODUCTION

Silk fibroin (SF) is one of the most promising biomaterials studied in recent years because of the performance of its mechanical properties, and also that it is environmentally friendly and biocompatible.[1] Through controlling the secondary structure of proteins, various morphologies of silk-based biomedical materials have been made, including tubes, sponge, hydrogel, fibers, and thin films.[2−7] Silk-based composite materials have also been fabricated with novel physical, chemical, and optical properties, which have been utilized in electrical and chemical fields.[8−11] However, many studies[2−4,12] have demonstrated that the water-based regenerated SF materials in the dry state are very brittle and rigid after crystallization and thus not suitable for many applications. The traditional water-based synthesis method is also very time-consuming, and the samples made by the process are initially water-soluble, requiring further treatments such as methanol annealing, water annealing, thermal treatment, and mechanical pressing[4,12−14] to induce insolubility through the formation of intermolecular β-sheet crystals. Therefore, a novel regeneration method to quickly induce both insolubility while retaining flexibility of SF materials is desired.

One potential option recently brought to attention is a formic acid (FA)-based fabrication method that has proven to be successful on *Bombyx mori* silk materials.[15−23] However, the utility of this method on the silk from other species has not been studied. In nature, Mori and Thai Bombyx silks, both produced by cultivated mulberry silkworms, have been used as luxurious textile commodities for centuries.[24−28] The white Mori silk comes from China, and the yellow Thai silk is from Thailand. Other silks from wild silkworms are often mechanically stiffer than that from the domesticated species. Dark tan Tussah silk is produced by *Antheraea mylitta*, light tan Muga silk comes from *Antheraea assamensis*, and Eri silk is from *Philosamia ricini*.[29] In the present research, we comparatively studied these five different types of regenerated silk protein films (Mori (China), Thai, Eri, Muga, and Tussah) produced by the formic acid-calcium chloride method, with a focus on the insolubility and flexibility. The function of calcium ions in these silk materials is also discussed, which can act as plasticizers to interact with the silk structure and prevent the molecules from forming stacked β-sheet crystals.

The FA regenerated films are water-insoluble and mechanically flexible in the dry state after direct solution casting, and no further physical or chemical treatments were needed for cross-linking. Using different methods, we comparatively demonstrate that the structural and physical properties of the original silk fibers (predominantly intermolecular β-sheet

Received: April 26, 2019
Accepted: October 24, 2019
Published: October 24, 2019

DOI: 10.1021/acsbiomaterials.9b00577
ACS Biomater. Sci. Eng. 2019, 5, 6361−6373

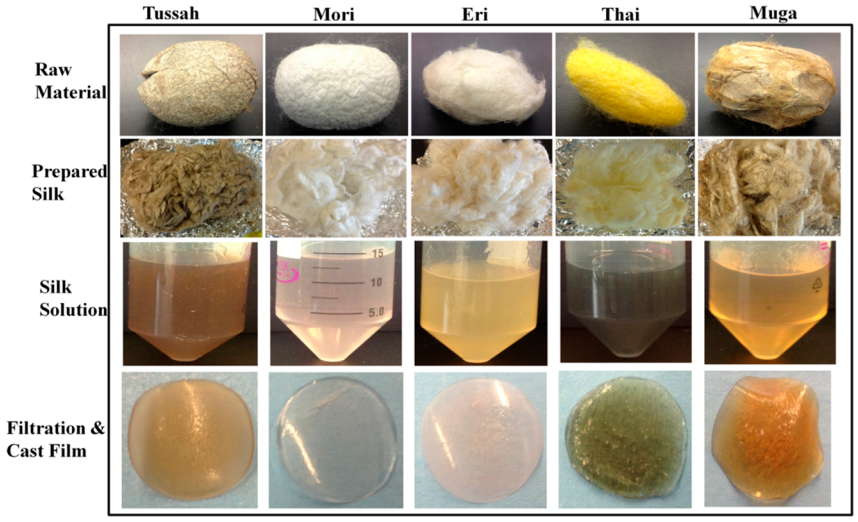

Figure 1. Processing of five different silkworm cocoons (top row) into silk fibroin films by the FA method. After the glue-like sericin proteins were removed (second row), silk fibroin fibers were dissolved into solution (third row), and then filtered and cast into regenerated films (bottom row).

crystals or silk II), water-based regenerated films (predominantly random coils or α-helix), and these FA-based regenerated films (predominantly intramolecular β-sheets or silk I) are completely different. Furthermore, the material properties, such as morphology, content of protein secondary structures, thermal and enzymatic stability, as well as mechanical properties of samples, are also investigated. A model is developed to explain the insolubility and flexibility mechanism of the regenerated films fabricated from this FA-based method, which can expand the potential applications of silk materials.

2. EXPERIMENTAL SECTION

2.1. Materials and Preparation. Silk cocoons of *P. ricini* (Eri), *A. assamensis* (Muga), and *A. mylitta* (Tussah) were obtained from India, while *B. mori* silkworm cocoons were obtained from China (denoted as Mori) and Thailand (denoted as Thai), separately. To remove the sericin coating on the silk fibers, the silkworm cocoons were first boiled in a 0.02 M $NaHCO_3$ (Sigma-Aldrich, U.S.) solution for 2 h and then rinsed thoroughly with deionized water three times. The details of the degumming procedure have been reported previously.[29,30]

After the SF fibers were obtained, two methods were used to generate silk films. One method was to gradually put the fibers into a mixture solution of formic acid (98%, MilliporeSigma) with 4 wt % calcium chloride ($CaCl_2$), and then continuously shake the solution until it dissolved at room temperature. The maximum concentration of silk samples in the FA-$CaCl_2$ solution is about 0.15 g/mL. The solution then was filtered with a syringe filter with 0.45 μm pore size (VWR International) to remove the impurities in the silk solution, after which the solution was centrifuged at 8000 rpm for 10 min to remove bubbles. Finally, the homogeneous solution was cast onto polydimethylsiloxane (PDMS) substrates at room temperature to form regenerated silk films. No gel formation was observed during the drying process. After 2 days of vacuum drying at room temperature, the formic acid was removed from the silk samples (verified by FTIR), and the regenerated silk films based on this FA-$CaCl_2$ method were produced. Films made this way are denoted by a suffix of FA. Figure 1 displays the appearances and shapes of five silks manufactured through the FA method at different processing stages.

The second method to obtain regenerated silk films was based on the traditional water-based procedure.[29] In general, the dried fibers were dissolved in a melted $Ca(NO_3)_2{\cdot}2H_2O$ (Sigma-Aldrich, U.S.) solution at 90 °C at a concentration of 10 wt %. The silk solution then was dialyzed by dialysis cassettes (Pierce Snake Skin MWCO 3500; Thermo Fisher Scientific Waltham, MA) against pH = 8–9 Milli-Q water for at least 2 days. Centrifugation was used to further remove small insoluble residues, and then SF aqueous solution with 6 wt % silk was obtained. Finally, the silk aqueous solutions were cast onto PDMS substrates and dried in a vacuum for 2 days to form the water-based silk fibroin films. Films synthesized in this fashion are denoted by a suffix of W.

2.2. Fourier Transform Infrared Spectroscopy (FTIR). FTIR analysis of silk samples was performed with a FTIR spectrometer (Tensor 27, Bruker, U.S.) with a deuterated triglycine sulfate detector and a multiple reflection, horizontal MIRacle ATR attachment with a Ge crystal (Pike Tech, Madison, WI). For each measurement, 128 scans were coded at a resolution of 4 cm^{-1} over the range 400–4000 cm^{-1}. Fourier self-deconvolution (FSD) of the IR spectra covering the amide I region (1595–1705 cm^{-1}) was performed with the Opus 5.0 software. Deconvolution was performed with Lorentzian line shapes with a half-width of 25 cm^{-1} and a noise reduction factor of 0.3, and the self-deconvoluted spectra were then subsequently fitted with Gaussian peaks, which were normalized by area to determine the fraction of the secondary structures in the silk films.[31]

2.3. X-ray Analysis. Wide-angle X-ray scattering (WAXS) was performed with a Panalytical Empyrean X-ray diffractometer. Silk fibers and films were mounted on an aluminum sample holder. The setup includes a fixed anode X-ray source for Cu Kα radiation (wavelength λ = 0.154 nm), operating at 45 kV and 40 mA. The scattering angle 2θ ranged from 5° to 40°, and data were taken in steps of 0.013° with a hold time of 30 s/step. The baseline was determined by subtracting the air background and fitted with a quadratic baseline as described previously.[32] The q vector was obtained from $q = 4\pi \times (\sin\theta)/\lambda$.

2.4. Scanning Electron Microscope (SEM). Surface morphology was characterized with a LEO ZEISS 1530 VP scanning electron microscope (Oberkochen, Germany). Silk film samples with a thickness of 1.0–1.2 mm were mounted onto a standard specimen holder with conductive carbon double-sided tape with the fracture surfaces toward the electron beam. The acceleration voltage was varied between 5 and 10 kV depending on the different imaging sizes and sample characteristics. To analyze the cross-sectional area of the silks, the samples were first quickly freeze-dried with liquid nitrogen to avoid deformation. They then were fractured in liquid nitrogen with a pair of tweezers and analyzed along the new surface.

2.5. Differential Scanning Calorimetry (DSC). Samples with masses about 6 mg were encapsulated in Al pans and heated in a differential scanning calorimeter (Q100, TA Instruments Co. Ltd., U.S.) with dry nitrogen gas flow of 50 mL min^{-1} and equipped with a refrigerated cooling system. Aluminum and sapphire reference

DOI: 10.1021/acsbiomaterials.9b00577
ACS Biomater. Sci. Eng. 2019, 5, 6361–6373

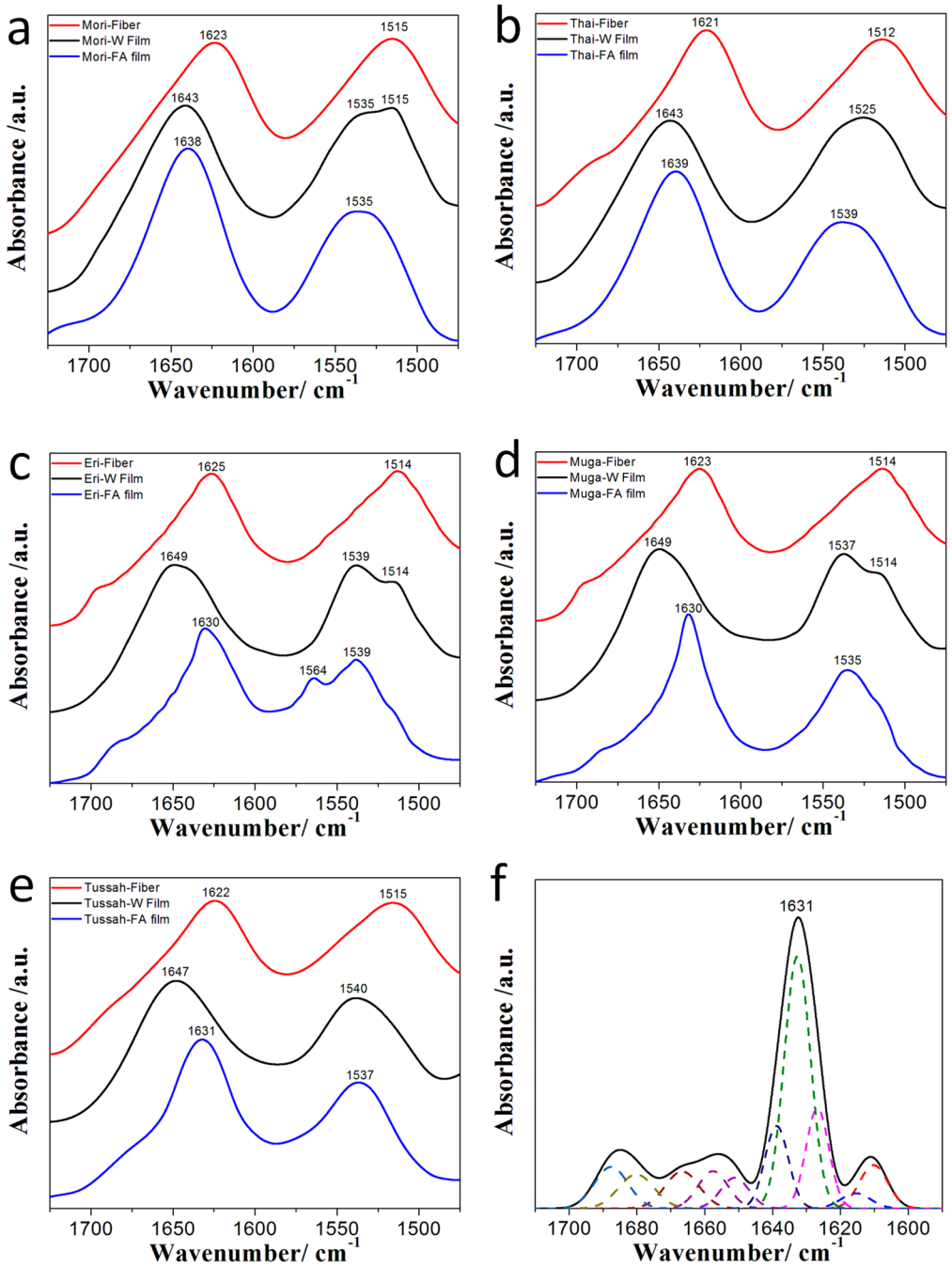

Figure 2. (a–e) FTIR absorbance spectra of different silk fibroin fibers and silk films regenerated from the formic acid method (FA) and the water method (W). (f) A curve-fitting example for FSD amide I spectra of a Tussah silk-FA film (centered at 1631 cm^{-1}). The fitted peaks are shown by dashed lines.

standards were used for calibration of the heat capacity through a three-run method described previously,[33] and the heat flow and temperature were calibrated with an indium standard. Standard mode DSC measurements were performed from −25 to 400 °C at a heating rate of 2 °C min^{-1}, while temperature-modulated differential scanning calorimetry (TM-DSC) measurements were performed at a heating rate of 2 °C min^{-1} with a modulation period of 60 s and temperature amplitude of 0.318 °C.

2.6. Thermal Gravimetric Analysis (TGA). Thermal gravimetric analysis (TGA) (Pyris 1, PerkinElmer Co. Ltd., U.S.) of regenerated silk-FA film samples was done with increasing temperature. Measurements were made under nitrogen atmosphere with a gas flow rate of 50 mL min^{-1} for temperatures ranging from ambient temperature to 450 °C at a heating rate of 5 °C min^{-1}.

2.7. Enzymatic Degradation. First, different silk films were cut into samples of mass 40 ± 5 mg. The films then were incubated at 37 °C in 40 mL of phosphate-buffered saline (PBS) solution containing 3.1 U mL^{-1} protease XIV, an enzyme used to analyze the biodegradation of the five silk samples. The buffer/enzyme solution was replaced daily so that the enzyme activity remained at a desired level throughout the entire experiment. The specimens were taken out and rinsed gently with distilled water three times and then weighed at room temperature until reaching constant mass.[34] For each type of silk film, at least seven samples were used to obtain a statistically significant result. Samples incubated in PBS solution without enzyme served as controls.

2.8. Mechanical Analysis. Static tensile experiments were performed with a dynamic mechanical analyzer (Diamond DMA,

DOI: 10.1021/acsbiomaterials.9b00577
ACS Biomater. Sci. Eng. 2019, 5, 6361–6373

Table 1. Percentages of Secondary Structures in Silk Protein Fibers and FA Regenerated Films, Calculated by a FTIR Deconvolution Method[a]

	intermolecular β-sheet	intramolecular β-sheet	random coils	α-helix	β-turn	side chain
Mori-FA film	16.9	20	34.7	8.4	14.9	5
Mori fiber	30.3	8.9	17.9	6.4	20.1	16.5
Thai-FA film	15.1	23	33.8	7.1	17.6	3.3
Thai fiber	30.1	9.9	16.3	5.8	17.4	20.5
Eri-FA film	23.1	29.4	13.1	5.6	19.0	9.8
Eri fiber	30.3	13.1	18.2	5.9	18.7	13.9
Muga-FA film	13.4	44.3	12.7	6.4	18.9	4.4
Muga fiber	31.4	14.8	18	5.7	22.2	8.9
Tussah-FA film	13.6	38.9	13.7	5.4	19.5	8.9
Tussah fiber	28	12.6	16.7	5.9	20.1	16.8

[a]All calculated secondary structure fractions have the same unit (wt %) with a ±2 wt % error bar.

Perkins-Elmer Instruments Co., U.S.) apparatus under SS pattern for silk-FA films. The shape of the film samples was rectangular, with a size of 5.0 mm × 6.0 mm and a thickness of 1.0−1.2 mm. The force was loaded from 5 to 4000 mN at 50 mN min^{-1} with the temperature maintained at ambient, and stress−strain curves were thus obtained.

3. RESULTS AND DISCUSSION

3.1. FTIR Analysis. FTIR analysis was performed to understand the structural differences of the five regenerated silk films. Figure 2a−e shows the FTIR absorbance spectra of different silk-FA films. For comparison, the spectra of the original SF fibers, as well as of silk-W films, are also shown in Figure 2. Generally, the IR spectral region between 1700 and 1600 cm^{-1} is assigned to the peptide backbone absorptions of the amide I (1700−1600 cm^{-1}) and amide II (1600−1500 cm^{-1}) regions.[35,36] The amide I region mainly comes from the C═O stretching vibrations (80%) of the protein backbones,[35] with minor contributions from the N−H in-plane bending, the out-of-phase C≡N stretching vibrations, and the C−C≡N deformation. Therefore, this region is the most commonly used for the quantitative analysis of protein secondary structures.[29] The amide II region is caused mainly by the out-of-phase combination of vibrations from the C−N stretching and the N−H in-plane bending. The microenvironment of protein side chain groups can easily affect this region.[29]

All silk samples showed two strong peaks in the amide I and amide II regions (Figure 2), indicating the presence of primary protein structures. The amide I (1600−1700 $cm^{-1)}$ region was then utilized to identify the secondary structures of silk materials. For the domestic Mori silk samples (Figure 2a), the peak of Mori fiber was centered at 1623 cm^{-1}, indicating mainly intermolecular β-sheet crystal structure. The peak of the Mori-FA film shifted to 1638 cm^{-1}, suggesting the presence of intramolecular β-sheet and random coil structures,[31,37−41] while the peak of Mori-W film was centered at 1643 cm^{-1}, indicating a large portion of random coils structure formed in the sample.

Similar results were also found for the Thai silk samples (Figure 2b). For Thai fiber, the peak was centered at 1621 cm^{-1} (intermolecular β-sheet structure). For Thai-FA film, it shifted to 1639 cm^{-1} (intramolecular β-sheet and random coil structures), and for Thai-W film it was centered at 1643 cm^{-1} (random coil structure).

The wild silk (Eri, Muga, and Tussah) samples shared similar features. The peak of Eri fiber was centered at 1625 cm^{-1} (intermolecular β-sheet structure), the peak of Eri-FA film shifted to 1630 cm^{-1} (intramolecular β-sheet structure), and the peak of Eri-W film was centered at 1649 cm^{-1} (α-helix/random coils). For Muga fiber, the amide I peak was centered at 1623 cm^{-1} (intermolecular β-sheet structure), while that of the Muga-FA film shifted to 1630 cm^{-1} (intramolecular β-sheet structure), and the peak of Muga-W was centered at 1649 cm^{-1} (α-helix/random coil structures). Last, the peak of Tussah fiber was centered at 1622 cm^{-1} (intermolecular β-sheet crystal structure), the peak of Tussah-FA film shifted to 1631 cm^{-1} (intramolecular β-sheet structure), and the peak of Tussah-W film was centered at 1647 cm^{-1} (α-helix/random coils). The structures of these wild silks are similar to each other where their intermolecular β-sheet content decreased during the FA-$CaCl_2$ dissolution process, while their intramolecular β-sheet content increased significantly. For all five types of silks, their peak positions in amide II region also shifted from being centered around 1512 cm^{-1} for silk fibers to higher wavenumber (centered around 1535 cm^{-1}, for silk-FA films).

Numerous studies have shown that secondary structures can significantly affect protein material properties. Schneider et al. reported that responsive hydrogels can be obtained through linking the intramolecular β-hairpin peptides.[42,43] Chen et al. proposed that the intramolecular β-sheets formed during the nucleation stage play a key role in the formation of silk nanofibers.[44] Du et al. reported that the less stable intramolecular β-sheet crystals, rather than the highly oriented rigid intermolecular β-sheet crystals, contribute to the high extensibility of spider silk.[45]

To quantify the percentage of the secondary structures in the regenerated silk samples, Fourier self-deconvolution was done for spectra in the amide I region (1595−1705 cm^{-1}).[31] Figure 2f shows an example of this FSD method on the amide I spectra of a Tussah silk-FA film. Table 1 lists the percentages of secondary structures in different silk fiber and FA film samples calculated by this deconvolution method. In general, the intermolecular β-sheet content of the silks decreased from that in the fiber form to that in the regenerated FA film, while the converse is true for the intramolecular β-sheet content. For example, intermolecular β-sheets of Mori silk decreased significantly from 30.3% (fiber) to 16.9% (FA film), and the intramolecular β-sheets largely increased from 8.9% (fiber) to 20% (FA film). Domestic Thai silk showed a similar trend, where intermolecular β-sheets decreased, and the intramolecular β-sheets increased from fiber to FA film. Meanwhile, the random coils content of Mori and Thai silk also increased more than 15% during the FA film regeneration process. For

DOI: 10.1021/acsbiomaterials.9b00577
ACS Biomater. Sci. Eng. 2019, 5, 6361−6373

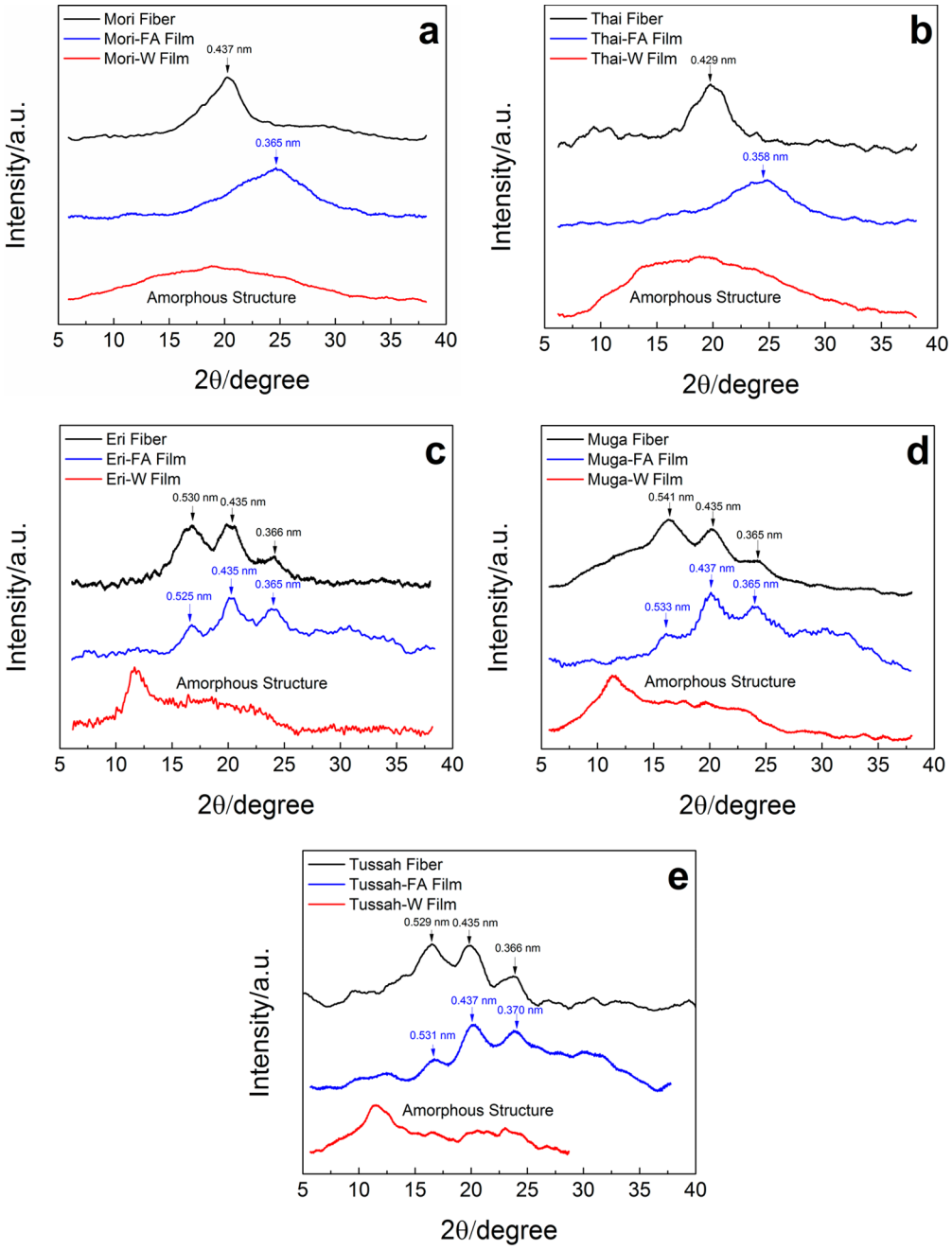

Figure 3. Wide-angle X-ray diffraction patterns of silk fibers, silk-FA films, and silk-W films: (a) Mori silk, (b) Thai silk, (c) Eri silk, (d) Muga silk, and (e) Tussah silk.

wild silk (Eri, Muga, and Tussah), likewise, the intermolecular β-sheet content was also reduced from fiber to FA film, while the intramolecular β-sheet content was greatly increased during the film formation. Interestingly, however, the relative amount of the random coil structure did not change significantly during regeneration.

These results indicate that the structures of silk fibers, silk-FA films, and silk-W films are significantly different from each other. As for the silk fibers, they are dominated by intermolecular β-sheets crystal structures, while silk-W films are dominated by random coils structures, resulting in the water solubility of the film samples. In contrast, silk-FA films show completely different behavior: during the dissolving process, the hydrogen bonds between the intermolecular β-sheet layers of silk fibers were destroyed by the $CaCl_2$-FA solution, while the content of intramolecular β-sheet increased, indicating that more intramolecular hydrogen bonds may be formed. Meanwhile, protein chains that did not form new hydrogen bonds would transfer to random coil structures under the influence of the FA-$CaCl_2$ solvents. Therefore, the intramolecular β-sheets and random coils were connected by remaining intermolecular β-sheets or calcium ions and formed a network, resulting in the insolubility of the cast silk-FA films. A model based on these results will be further described in the Assembly Mechanism section.

3.2. WAXS Analysis. To further understand the results, WAXS was used to investigate the crystal structures of silk fibers and films regenerated from different methods (Figure 3).

DOI: 10.1021/acsbiomaterials.9b00577
ACS Biomater. Sci. Eng. 2019, 5, 6361−6373

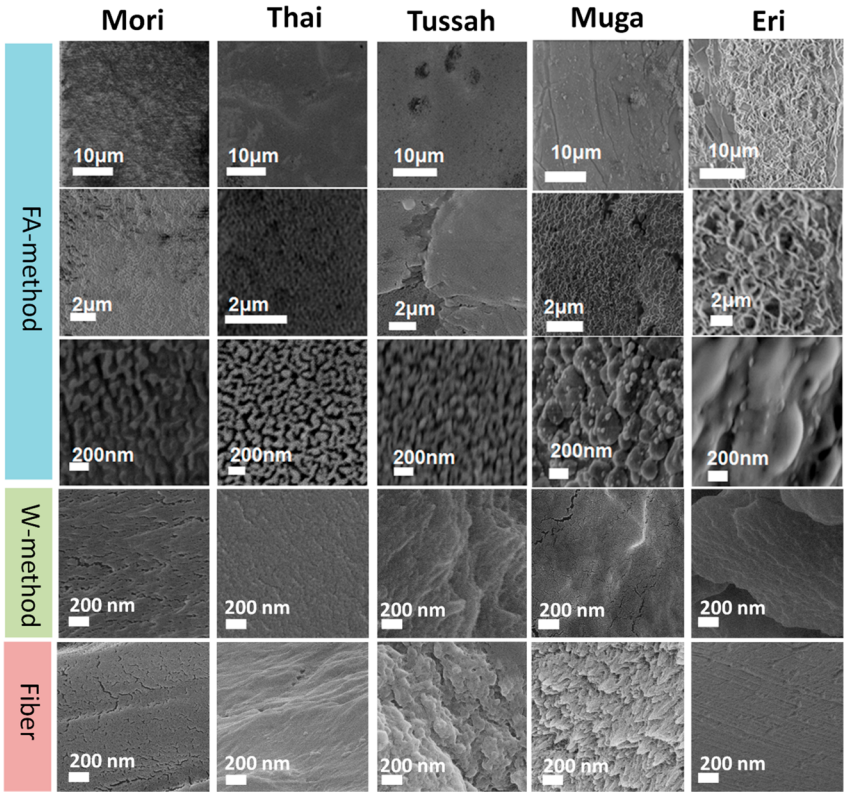

Figure 4. SEM images of different types of silk-FA films, silk-W films, and native fibroin fibers at cross-section area.

The predominant WAXS peak positions of silk-FA films, silk-W films, and natural silk fibroin fibers are summarized in Table S1. The WAXS data indicate that both domestic silk fibers (Mori and Thai) and wild silk fibers (Eri, Muga, and Tussah) have similar internal crystal structures. In Figure 3a, Mori fiber shows a peak at 20.3° (lattice spacing d = 0.437 nm), suggesting a typical β-sheet crystal dominated silk II structure.[15,46−48] In Figure 3b, Thai fiber also shows a peak at 20.4° (d = 0.435 nm, silk II), which correlates well with the FTIR data that silk fibers were dominated by intermolecular β-sheet crystal structures. In contrast, Mori-FA film and Thai-FA film both show a broad peak centered at 24.3° (d = 0.365 nm) and 24.8° (d = 0.358 nm), respectively, which is typically correlated with the silk I structure.[48]

The silk I structure is the precursor structure of silk II crystals, found in silkworm glands just before the fiber spinning.[49] Previously, several studies have reported the fabrication of silk I materials, which can provide significantly improved flexibility to the samples.[4,15,50] According to the FTIR results, it is suggested that Mori and Thai films manufactured by the FA method are dominated by intramolecular β-sheets. Because intramolecular β-sheet structure may be an intermediate stage from ordered α-helix structure to stacked compact intermolecular β-sheet crystal structures,[49] the WAXS data indicate that Mori and Thai FA films are in a late-stage silk I or early-stage silk II structure, where most of the α-helix structures have transformed to the denser intramolecular β-sheet structures but are still not close enough to form β-sheet crystals. The high content of intramolecular β-sheets in FA films resulted in better flexibility, similar to that of the ordered α-helix structures.

As compared to the Mori-FA and Thai-FA films, Mori-W and Thai-W films both demonstrated apparent broad amorphous halo peaks centered around 16−20°, indicating that random coil structures dominate in the water regenerated films. The amorphous structure also accounts for the solubility of the silk-W films.[51]

The three types of wild silk fibers show similar results. For the fiber samples, Eri fiber has three peaks at 16.6° (d = 0.530 nm, silk II), 20.4° (d = 0.435 nm, silk II), and 24.3° (d = 0.366 nm, silk I).[52−54] Muga fiber also has three peaks at 16.4° (d = 0.541 nm, silk II), 20.4° (d = 0.435 nm, silk II), and 24.4° (d = 0.365 nm, silk I).[52−54] For Tussah fiber, the three peaks are centered at 16.7° (d = 0.529 nm, silk II), 20.4° (d = 0.435 nm, silk II), and 24.3° (d = 0.366 nm, silk I).[52,53] It confirms that these three types of wild silk fibers have more ordered structures than the two domestic silk fibers, as we suggested previously.[33] Those three types of wild silk fiber possess better mechanical properties than the domesticated ones likely due to their higher content of intermolecular and intramolecular β-sheets (Table 1).

For the regenerated Eri-FA, Muga-FA, and Tussah-FA films, there were also three prominent X-ray peaks. However, their relative intensities and positions are different from those of their respective fibers. For Eri-FA film, the three peaks are centered at 16.6° (d = 0.533 nm, silk II), 20.4° (d = 0.435 nm, silk II), and 24.0° (d = 0.370 nm, silk I).[52−54] As compared to the Eri fiber, the relative intensity of the silk II peak centered at 16.8° decreased significantly, while that of the silk I peak centered at 24.3° (Eri fiber) increased and slightly shifted slightly, indicating the formation of additional silk I structure.[52−54] Because it has been confirmed by FTIR that the content of intermolecular β-sheets drops while the amount of intramolecular β-sheets increases during this FA-based regeneration process, it is believed that $CaCl_2$-FA system first destroyed the hydrogen bonds within the intermolecular β-

DOI: 10.1021/acsbiomaterials.9b00577
ACS Biomater. Sci. Eng. 2019, 5, 6361−6373

sheet crystals in silk fibers, and then the released silk chains self-assembled through intramolecular hydrogen bonds forming intramolecular β-sheets. The mechanism of assembly in Eri-silk films is the same as that in the domestic silk-FA films, that is, the formation of late-stage silk I or early-stage silk II structures.

There are similar results for the Muga-FA and Tussah-FA films. WAXS shows three peaks, which are located at 16.9° (d = 0.531 nm, silk II), 20.3° (d = 0.437 nm, silk II), and 24.0° (d = 0.370 nm, silk I) for the Muga-FA film, and likewise three peaks located at 16.8° (d = 0.531 nm, silk II), 20.4° (d = 0.435 nm, silk II), and 24.0° (d = 0.370 nm, silk I) for the Tussah-FA film. In contrast, all three types of wild silk-W films show similar amorphous and α-helix (2θ = 11.7°) peaks.[55]

3.3. SEM Analysis. The cross-sectional morphologies of five different silk-FA films, silk-W films, and their native fibroin fibers were obtained by SEM (Figure 4). Alignment of the nanofibril structures can be seen clearly on the 2 μm and 200 nm scales for all silk-FA films.[56] Also, the nanofibril structures vary in length and shape (rod, "S", circular, etc.) for different silk-FA films. For the Mori silk-FA films, the cross-section appears uniform on the 10 μm scale, apart from random nanofibril structures. On the 2 μm scale, the areas become rougher, but no significant structural components can be identified from this scale. On the 200 nm scale, globular structures appeared, which are typical morphological components of Mori silk molecular aggregates found in previous studies.[29] On the 10 μm scale, the cross-section area of Thai silk-FA film appears smooth with patches of roughness, which becomes more prevalent at the 2 μm scale. On the 200 nm scale, the silk structure is clearly seen as globular shaped, similar to that of Mori silk-FA film. The Tussah silk-FA film shown on the 10 and 2 μm scales is random in shape but appears to be more aligned than the randomly dispersed Thai silk-FA in the 200 nm scale. For the Muga silk-FA sample, at the 10 μm scale, the cross-section appears solid with scattered cracks. Pellets appear scattered as well. Upon a 2 μm scale examination, the cross-section is composed of numerous globular structures. These globules appear in size and shape similar to smaller pellets present between globules. At the 200 nm scale, globule sizes are less similar, and smaller particles are more visible. As for the Eri silk-FA sample, the cross-section is flaky in appearance in the 10 μm scale, and there are obvious layers in the structure. Shown on the 2 μm scale, the flaky appearance is less sharp and defined. At the 200 nm scale, globular components are prevalent, and the laminar structure can no longer be seen. As compared to silk-FA films, the nanostructure features of silk-W films and silk fibroin fibers at 200 nm (Figure 4) are not obvious except for the Tussah and Muga fibers.

3.4. DSC Analysis. Figure 5a shows the standard DSC scans of various silk-FA film samples. During heating scans, all samples first showed a low-boiling bound solvent evaporation peak T_{d1}[33] around 60−100 °C (333−373 K). Table 2 shows that the trend of the temperature of this peak is Mori-FA < Thai-FA < Eri-FA < Muga-FA < Tussah-FA, where the T_{d1} of Tussah-FA film was the highest temperature found in all silk samples. Similar to the silk-W films we reported previously,[29] the T_{d1} values of the three wild silk samples were higher than those of the two domesticated ones, indicating that wild silks are better at maintaining bound molecules in their structures. For the wild (Muga, Eri, and Tussah) silkworms, this silk structure could be more favorable for their surviving in the wild

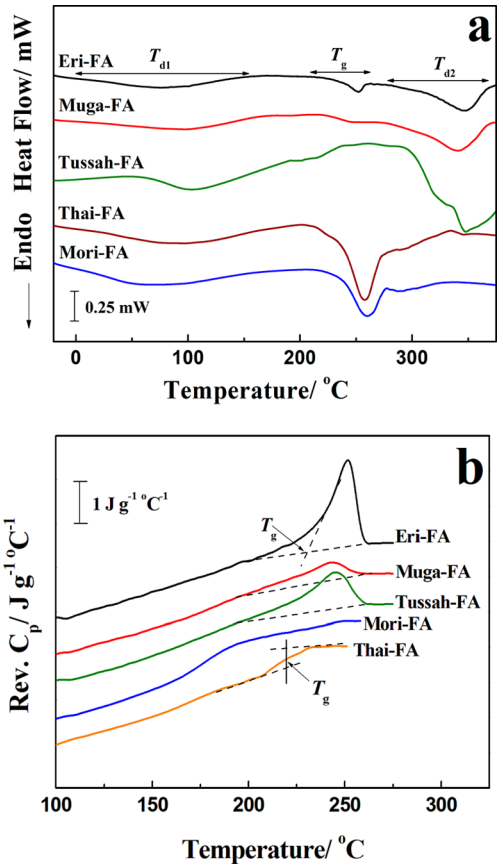

Figure 5. (a) Standard DSC scans of five silk films (Tussah-FA, Mori-FA, Eri-FA, Thai-FA, and Muga-FA) prepared by the FA method, with temperature regions related to bound solvent evaporations (T_{d1}), glass transitions (T_g), and sample degradations (T_{d2}). (b) The reversing heat capacities of the five silk film samples prepared by the FA method, measured by TMDSC from 100 to 275 °C (glass transition region), with a 2 °C min^{-1} heating rate, a modulation period of 60 s, and a temperature amplitude of 0.318 °C.

environment. However, the T_{d1} values of all silk-FA samples were generally lower than those of silk-W films. This implied that the FA-$CaCl_2$ solution may have affected their water inhibition or reservation ability during the dissolving process.

For temperatures above the T_{d1} region, the glass transition temperature T_g and the degradation temperature T_{d2} region of various silk films can be seen in Figure 5a. Near T_g regions, all silk-FA films showed clear heat capacity increases ΔC_p as found in their TMDSC curves (Figure 5b), which are used to investigate the reversible thermal properties of silk film materials. All samples showed clear heat capacity increases ΔC_p in their T_g regions. Interestingly, for wild silk films synthesized by the FA method, there was an endothermal peak occurring with the ΔC_p step change in the T_g region, while domesticated silk films (Mori and Thai) only show a simple ΔC_p step occurring in the T_g region. The endothermal peak found in the wild silk T_g region may be associated with the physical relaxation process of wild silk molecular chains during the heating progress.[57] Thus, the midpoint temperature of this transition for domesticated silk films (Thai, Mori) was chosen as T_g, while the onset temperature was used for the T_g values of wild silk samples (Muga, Tussah, and Eri) in this study.[58,59] Table 2 lists the T_g of various silk samples and their ΔC_p values during the glass transition. For silk films manufactured by the

DOI: 10.1021/acsbiomaterials.9b00577
ACS Biomater. Sci. Eng. 2019, 5, 6361−6373

Table 2. Thermal Analysis Data of Different Silk Protein Films Produced by the FA Method[a]

silk sample	T_g/°C	ΔC_p at T_g/ J g^{-1} K^{-1}	solvent release T_{d1}/°C	degradation temp T_{d2}/°C	onset temp of decomposition/°C	bound solvent content/%	degradation middle temp T_{dm}/°C	remainingmass at 400 °C/%
Eri	238.8^F/176.0^W	0.041^F/0.509^W	84.5^F/119.0^W	346.2^F/329.0^W	327.0	6.84	372.7	47.42
Muga	232.4^F/168.0^W	0.135^F/0.370^W	95.3^F/120.3^W	341.8^F/330.3^W	384.8	5.99	396.6	49.24
Tussah	233.9^F/188.0^W	0.019^F/0.282^W	103.2^F/131.6^W	348.2^F/336.6^W	319.1	6.43	375.3	49.26
Thai	217.8^F/149.0^W	0.388^F/0.564^W	78.2^F/96.2^W	258.1^F/245.4^W	306.0	12.33	328.3	54.06
Mori	176.3^F/175.0^W	0.483^F/0.475^W	74.5^F/112.7^W	260.3^F/244.3^W	300.3	10.09	313.8	26.32

[a]All numbers have an error bar within ±5%. The first four columns (T_g, ΔC_p at T_g, T_{d1}, and degradation T_d) were determined by DSC and TMDSC analysis, while the rest were determined by TG analysis (silk-FA films only). T_g, T_{d1}, and T_{d2} represent the glass transition temperature, bound solvent release peak temperature, and degradation peak temperatures of different silk-FA films, where the superscript "F" indicates results from the samples manufactured by the formic acid-$CaCl_2$ method and "W" represents samples manufactured by the water-based method.[29]

FA method, it showed a T_g trend of Mori < Thai < Muga < Tussah < Eri. It should be noted that the T_g values of the domestic silks are lower than those of the wild ones.

In contrast, the heat capacity increments ΔC_p at T_g of Mori and Thai films are higher than those of wild silk samples, with a ΔC_p trend of Tussah < Eri < Muga < Thai < Mori. For the Mori film sample, the ΔC_p increment at T_g was 0.483 J kg^{-1} °C^{-1}, which is close to our previous result obtained from the Mori-W films.[29] The Thai-FA film showed a similar ΔC_p increment (0.388 J kg^{-1} °C^{-1}) at T_g because it also belongs to the domestic silkworm species. The ΔC_p of Tussah sample was 0.019 J kg^{-1} °C^{-1}, which was the lowest among all silk samples. The ΔC_p is directly proportional to the average chain mobility of proteins, reflecting the number of freely rotating bonds capable of changing the chain conformation. In addition, T_g values of all silk-FA samples are higher than those of silk-W films (Table 2),[29] while their ΔC_p values are lower.[29] These results again prove that the FA method could make the protein chains arrange in a more ordered structure such as intramolecular β-sheet structure as compared to the silk-W samples.

Above T_g, all samples start to thermally degrade (Figure 5a).[59] Table 2 lists the T_{d2} values of all silk-FA films, with an order of Thai < Mori < Muga < Eri < Tussah. It is clearly shown that the T_{d2} values of domestic silk-FA films (282.2 and 284.7 °C, respectively) were significantly lower than those of wild silk-FA films (Figure 5a), indicating that wild silk protein films are more thermally stable than domesticated silk protein films, which is consistent with our previous conclusions.[29]

3.5. Thermal Stability.

Figure 6a shows the mass percentage change of Thai, Mori, Eri, Tussah, and Muga silk-FA films during a heating scan from room temperature to 450 °C, while Figure 6b shows the temperature derivative of their respective mass percentage curves. The bound solvent/water content (T_w), onset temperature of decomposition (T_d), middle degradation temperatures (T_{dm}), and the remaining mass at 400 °C of different silk-FA films are summarized in Table 2.

During the initial heating from room temperature to 150 °C, bound solvent/water molecules were first removed from all silk-FA samples, as demonstrated in the DSC study (T_{d1}). Table 2 lists the solvent content (%) of various silk-FA films measured by TGA. It shows that all samples contained bound solvent/water around 5.9−12.4%, with a trend of Muga < Tussah < Eri < Mori < Thai, with domesticated silk films showing larger values than those of the wild silks. Dehydration of bound solvent/water in domestic silks is much easier than it is in the wild silks, as was seen in the DSC study. The dehydration step in the TGA curve (Figure 6a) corresponds to

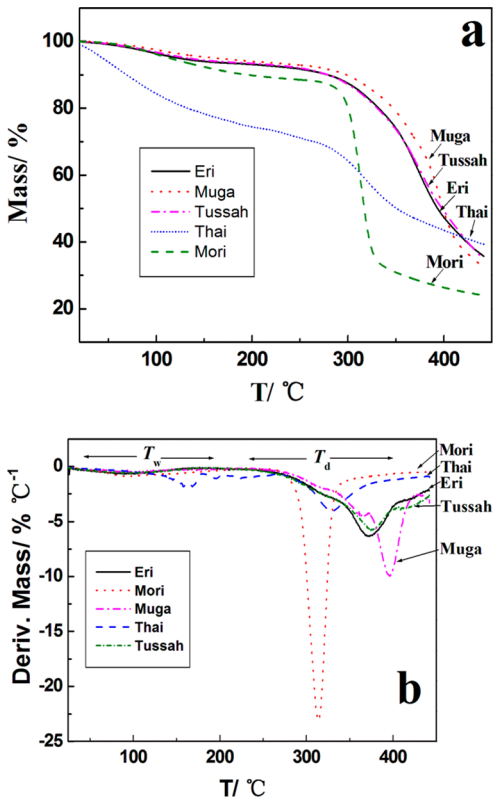

Figure 6. (a) Percent mass remaining of different FA-based silk fibroin film samples measured by thermogravimetric analysis during heating from room temperature to 450 °C at 5 °C min^{-1}. (b) The first derivative of the percent mass remaining in (a), which reveals the degradation rates of silk films and demonstrates temperature regions related to bound solvent/water evaporations (T_w) and the sample degradations (T_d).

a small peak in the differential thermogravimetric curve (Figure 6b), while the initial decomposition of the silk proteins started around 300 °C (Figure 6a). Figure 6b also shows that some wild silk samples (Muga and Eri) had a very quick mass loss during their major degradation stages, while the T_{dm} values of the two domesticated silks were lower than those of all wild silks, with a T_{dm} trend of Mori < Thai < Eri < Tussah < Muga (Table 2). The trend of middle degradation temperatures confirmed that wild silk-FA films are more robust than the domesticated films, as suggested by the DSC study. The remaining mass (%) of all samples at 400 °C was also listed in Table 2. For the Mori silk samples, the remaining mass was 26.32% at 400 °C, which is the lowest content among all film

DOI: 10.1021/acsbiomaterials.9b00577
ACS Biomater. Sci. Eng. 2019, 5, 6361−6373

samples, suggesting that the thermal stability of Mori film in high temperature regions is weaker than that of others. The Eri, Tussah, and Muga silks showed very similar decomposition curves with about 50% of the mass lost by 400 °C.

Previously, we have investigated the thermal properties of all silk-W samples by DSC.[29] As compared to those of the silk-W samples, the solvent release temperature and the thermal degradation temperature of silk-FA samples were much higher, especially for the wild silk types. This implies that the FA method increases the thermal stability of silk materials, perhaps through enhancing intramolecular β-sheet content in the structure.

3.6. Enzymatic Degradation. Enzymatic degradation of silk-FA films was studied in vitro. Figure 7 shows the weight losses of five silk-FA films in PBS solutions (Figure 7a) and protease XIV enzyme solutions (Figure 7b). For comparison, Figure 7c also shows the weight losses of five silk-W films in the protease XIV enzyme solutions (precrystallized by 30 min pure methanol treatment). During the first 5 h, the degradation rate appeared to be quicker, with a trend of Tussah < Thai < Eri < Muga < Mori, due to the degradation of nanocrystalline components in the films. As compared to other silk samples, the Thai silk sample continue to degrade quickly up to 20 h (similar to its TGA thermal degradation trend at low temperature region in Figure 6a), whereas the degradation rate of other silk samples tended to significantly slow after 5 h. The Tussah sample degraded only ~10% after 20 h of protease XIV enzymatic treatment. After 30 h, the degradation of silk films reached a quasi-equilibrium state, suggesting that β-sheet structures (intra- and intermolecular) can prohibit the enzymatic degradation of silk materials very well.[4,34,51,60,61] Their degradation profiles followed a clear trend of Tussah < Eri < Muga < Mori < Thai. It also demonstrated that the wild silk samples were more stable in the protease as compared to the domestic silk samples, probably due to the larger amount of β-sheet structures in the wild silk-FA samples as seen from FTIR.

However, for the pure methanol cross-linked silk-W films (Figure 7c), after 45 h, the degradation of Thai, Mori, Tussah, and Eri was significant with only about 10−15% of the original mass left. The MeOH cross-linked Muga-W was an exception, showing the lowest degradation rate (85% mass remaining) in all silk samples. In general, it is shown that the enzymatic degradation rate of methanol cross-linked silk-W films is much quicker than that of silk-FA samples. Because it has been widely proved that methanol can induce ~50% β-sheet structures (intra- and intermolecular β-sheets in total) in the regenerated water-based silk materials,[4,50,62] which is similar to the silk-FA samples, this result also indicates that not only the amount of β-sheet structures contributes to the stability of silk materials in enzymes, but also the size, pattern, or distribution of β-sheet structures in silk materials could be critical to help the protein molecules against enzyme digestions for a long time.

3.7. Mechanical Properties. Figure 8 shows the stress−strain curves of different silk-FA films, and Table 3 lists their elastic modulus, strength of extension, and elongation ratio calculated from the strain−stress curves. For the five silk-FA films, the trend of elastic modulus is Eri > Tussah > Muga >

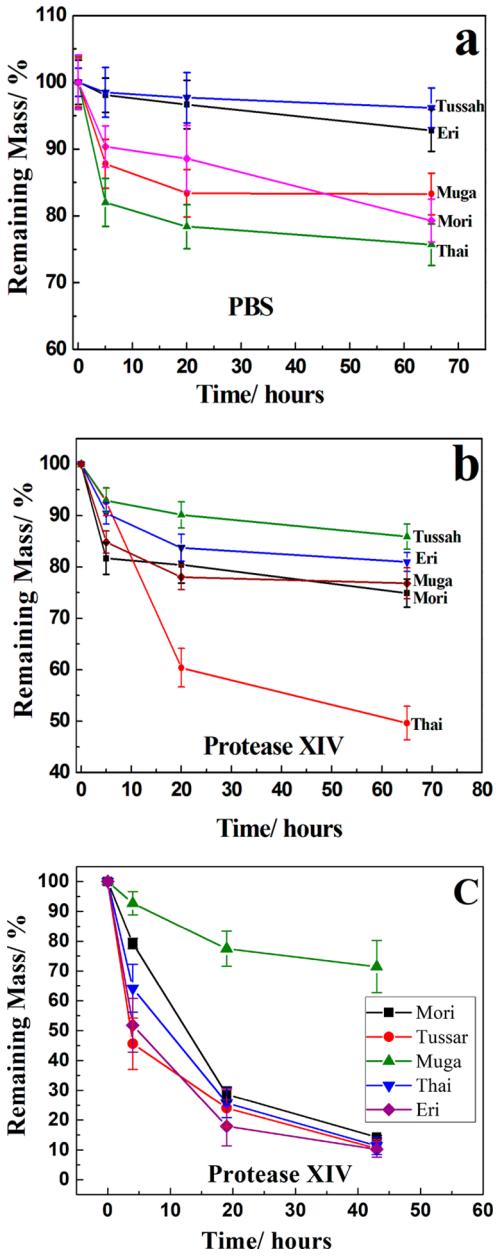

Figure 7. (a) PBS solution degradation and (b) protease XIV enzymatic degradation study of silk-FA films, and (c) protease XIV enzymatic degradation of silk-W films precrystallized by methanol.

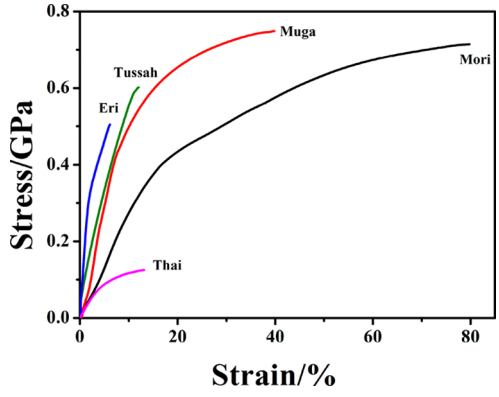

Figure 8. Stress−strain curves of different silk-FA samples (Tussah-FA, Muga-FA, Eri-FA, Mori-FA, and Thai-FA) measured by the static tensile test using DMA.

DOI: 10.1021/acsbiomaterials.9b00577
ACS Biomater. Sci. Eng. 2019, 5, 6361−6373

Table 3. Mechanical Properties of Silk-FA Films by DMA (Sample Size n = 5)

sample	elastic modulus (GPa)	strength of extension (GPa)	elongation (%)
Tussah	5.797 ± 0.406	0.602 ± 0.042	12.12 ± 0.82
Muga	5.658 ± 0.458	0.749 ± 0.060	39.83 ± 2.79
Eri	18.712 ± 1.16	0.502 ± 0.031	6.11 ± 0.35
Mori	2.573 ± 0.129	0.716 ± 0.034	79.72 ± 3.83
Thai	2.236 ± 0.094	0.125 ± 0.005	13.11 ± 0.60

Mori > Thai, and their strength of extension trend is Muga > Mori > Tussah > Eri > Thai, while the elongation ratio trend is Mori > Muga > Thai > Tussah > Eri. It shows that the Eri sample has the largest modulus and a high tensile strength but the lowest elongation. The Mori sample was soft and tough, with a lower modulus and the highest elongation, while the Thai film sample had a low strength of extension, although it had the lowest modulus among them. Both Muga and Tussah silk films fabricated from the FA method have relatively high strengths of extension and elongation ratios. As compared to data on crystallized insoluble water-based silk films,[63,64] the silk FA films are softer with higher elastic modulus and larger elongation ratio, which can be used for large deformation of materials in the future.

3.8. Assembly Mechanism. To elucidate the mechanism of assembly and water insolubility of silk-FA films, a schematic model is proposed in Figure 9. As shown in Figure 9, silk-W films regenerated from silk fibers (Figure 9a) are random coils dominated with only a little amount of α-helix and intramolecular β-sheets (Figure 9c).[29] It has been well-studied that these noncrystalline amorphous structures resulted in the water solubility of silk-W films (Figure 9c).[4,51] Two methods are generally used to induce insolubility of the silk-W films: (i) an annealing or preaggregation procedure (low temperature water annealing,[50,65] a repeated concentrating−dissolving procedure in solution,[66] self-assembly in silkworm glands,[67,68] etc.) can cause the noncrystalline structure to transfer to an early stage of silk I structure, with a high content of α-helix and intramolecular β-sheet;[4,51] (ii) the use of organic solvents (MeOH, EtOH, etc.), salts, mechanical pressing, or thermal treatments can make the silk noncrystalline structure transform back into the silk II structure (Figure 9a) with a large amount of intermolecular β-sheet crystals.[50,67,68]

On the basis of our previous results, it is believed that the $CaCl_2$-FA solvent system can directly disrupt the intermolecular cohesive force within the intermolecular β-sheet crystals in the SF fibers. Formic acid and $CaCl_2$ molecules functioned as plasticizers in this system, and the stacked intermolecular multilayer β-sheet crystals (silk II) within the highly crystallized natural silk fibers were quickly exfoliated into single layer intramolecular β-sheets or even random coils. Thus, the silk fibers were totally dissolved into the $CaCl_2$-FA system forming a homogeneous fibroin solution. During the drying process, with the evaporation of the formic acid, the fibroin fibers assembled together into nanofibrils with dominated intramolecular β-sheet structures (Figure 9b). The function of calcium ions (Ca^{2+}) in silk materials has been studied previously.[15,69] Furthermore, it has been demonstrated that Ca^{2+} ions can strongly interact with the silk structure in solution and prevent the molecules from forming intermo-

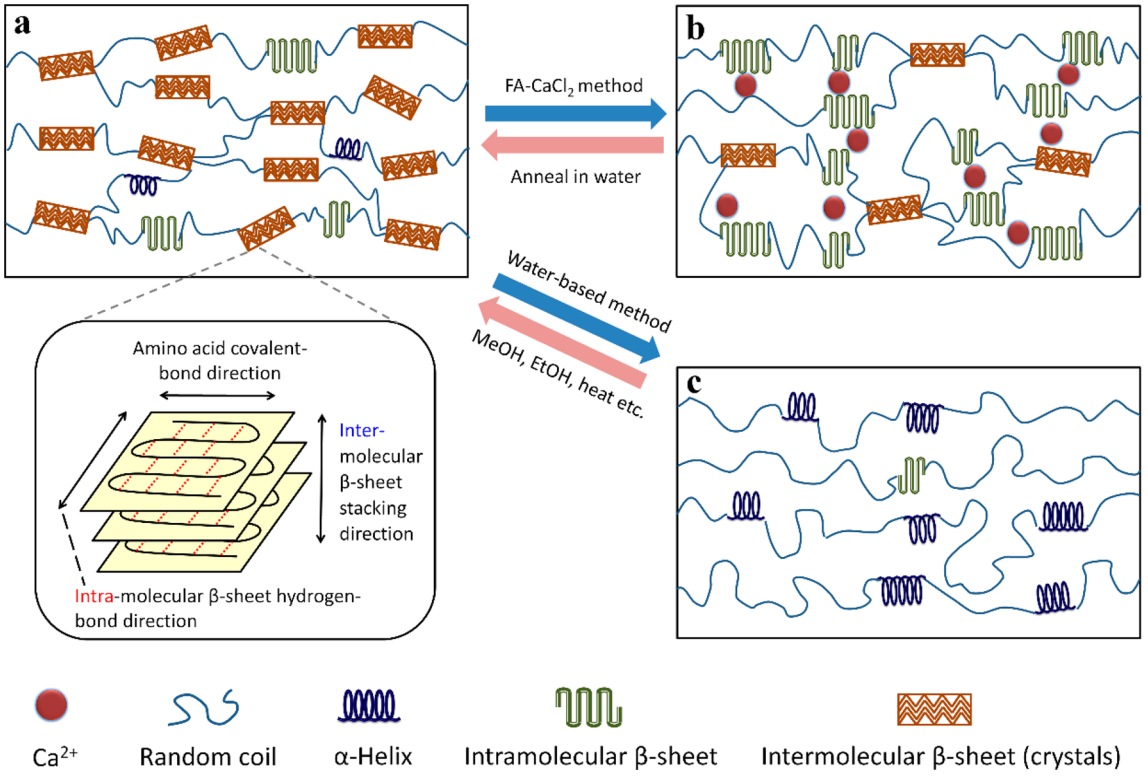

Figure 9. Structure models of silk fibers and films: (a) large amount of intermolecular β-sheets (crystals) and less amount of intramolecular are connected by random coils, silk II structure, forming the stable property of silk fibers; (b) large amount of intramolecular β-sheets and less amount of intermolecular β-sheets are connected by random coils forming a stable network, causing the insolubility of silk-FA films; and (c) a little amount of α-helix and tiny amount of intramolecular β-sheets are connected by the random coils, forming the amorphous structure of silk-W films.

DOI: 10.1021/acsbiomaterials.9b00577
ACS Biomater. Sci. Eng. 2019, 5, 6361−6373

lecular β-sheet crystals (Figure 9b).[15,69] Therefore, with the help of calcium ions as plasticizers, the cast silk-FA films show a structure dominated with intramolecular β-sheets instead of a large amount of intermolecular β-sheet crystals. Our results suggest that the intramolecular β-sheets not only provide additional flexibility to the system (as compared to intermolecular β-sheet crystals), but also result in the water insolubility of the silk-FA films. Because this structure is very close to the silk I structure found in WAXS patterns, we believe it is a late-stage silk I structure or the silk II precursor structure in the silk materials. In fact, upon long-time annealing in aqueous solution, the structure does transfer to silk II β-sheet crystal structure in the films.

4. CONCLUSION

This study presents a mechanism study on the structure and insolubility of the silk materials from five different species regenerated from a formic acid-$CaCl_2$ method. It reveals that the secondary structures of silk-FA films are different from those of their natural silk fibroin fibers, which are typically dominated by stacked intermolecular β-sheet crystals. In addition, the intramolecular β-sheet content of the silk-FA films is much higher than that regenerated from the traditional water-based method, causing silk-FA films to become insoluble in water. These results show that the intermolecular hydrogen bonds within β-sheets crystals in the silk fibers can be quickly disrupted during the dissolving process and allow a film network structure dominated by intramolecular β-sheets to form. From these observations, a model was proposed to explain the mechanism of assembly for the silk-FA films. This comparative study offers important insight into how to manipulate the secondary structures of silk-based biomaterials to tune its properties.

■ ASSOCIATED CONTENT

Supporting Information

The Supporting Information is available free of charge on the ACS Publications website at DOI: 10.1021/acsbiomaterials.9b00577.

Table S1 and additional references (PDF)

■ AUTHOR INFORMATION

Corresponding Author

*Phone: (856) 256-4860. Fax: (856) 256-4478. E-mail: hu@rowan.edu.

ORCID

Xiao Hu: 0000-0002-2579-2820

Author Contributions

⊥Y.X. and F.W. contributed equally to this work.

Funding

This study was supported by the Rowan University Start-up Grants. X.H. is also supported by the US NSF Biomaterials Program (DMR-1809541) and Materials Engineering and Processing Program (CMMI-1561966). F.W. is also supported by the National Natural Science Foundation of China (21973045).

Notes

The authors declare no competing financial interest.

■ ACKNOWLEDGMENTS

We would like to thank Jethro Medina for his initial suggestions for this study.

■ REFERENCES

(1) Hu, X.; Cebe, P.; Weiss, A. S.; Omenetto, F.; Kaplan, D. L. Protein-based composite materials. *Mater. Today* **2012**, *15* (5), 208–215.

(2) Bai, L. Q.; Zhu, L. J.; Min, S. J.; Liu, L.; Cai, Y. R.; Yao, J. M. Surface modification and properties of Bombyx mori silk fibroin films by antimicrobial peptide. *Appl. Surf. Sci.* **2008**, *254* (10), 2988–2995.

(3) Vepari, C.; Kaplan, D. L. Silk as a biomaterial. *Prog. Polym. Sci.* **2007**, *32* (8–9), 991–1007.

(4) Lu, Q.; Hu, X.; Wang, X.; Kluge, J. A.; Lu, S.; Cebe, P.; Kaplan, D. L. Water-insoluble silk films with silk I structure. *Acta Biomater.* **2010**, *6* (4), 1380–7.

(5) Chao, P. H.; Yodmuang, S.; Wang, X.; Sun, L.; Kaplan, D. L.; Vunjak-Novakovic, G. Silk hydrogel for cartilage tissue engineering. *J. Biomed. Mater. Res., Part B* **2010**, *95* (1), 84–90.

(6) Shen, W. L.; Chen, X. A.; Chen, J. L.; Yin, Z.; Heng, B. C.; Chen, W. S.; Ouyang, H. W. The effect of incorporation of exogenous stromal cell-derived factor-1 alpha within a knitted silk-collagen sponge scaffold on tendon regeneration. *Biomaterials* **2010**, *31* (28), 7239–7249.

(7) Wang, F.; Chandler, P.; Oszust, R.; Sowell, E.; Graham, Z.; Ardito, W.; Hu, X. J. J. o. T. A. Calorimetry, Thermal and structural analysis of silk–polyvinyl acetate blends. *J. Therm. Anal. Calorim.* **2017**, *127* (1), 923–929.

(8) Kang, M.; Jin, H. J. Electrically conducting electrospun silk membranes fabricated by adsorption of carbon nanotubes. *Colloid Polym. Sci.* **2007**, *285* (10), 1163–1167.

(9) Hronik-Tupaj, M.; Raja, W. K.; Tang-Schomer, M.; Omenetto, F. G.; Kaplan, D. L. Neural responses to electrical stimulation on patterned silk films. *J. Biomed. Mater. Res., Part A* **2013**, *101* (9), 2559–72.

(10) Wang, F.; Jyothirmayee Aravind, S. S.; Wu, H.; Forys, J.; Venkataraman, V.; Ramanujachary, K.; Hu, X. Tunable green graphene-silk biomaterials: Mechanism of protein-based nanocomposites. *Mater. Sci. Eng., C* **2017**, *79*, 728–739.

(11) Vu, T.; Xue, Y.; Vuong, T.; Erbe, M.; Bennet, C.; Palazzo, B.; Popielski, L.; Rodriguez, N.; Hu, X. Comparative Study of Ultrasonication-Induced and Naturally Self-Assembled Silk Fibroin-Wool Keratin Hydrogel Biomaterials. *Int. J. Mol. Sci.* **2016**, *17* (9), 1497.

(12) Jin, H.-J.; Park, J.; Valluzzi, R.; Cebe, P.; Kaplan, D. L. Biomaterial Films of Bombyx M ori Silk Fibroin with Poly (ethylene oxide). *Biomacromolecules* **2004**, *5* (3), 711–717.

(13) Jin, H. J.; Kaplan, D. L. Mechanism of silk processing in insects and spiders. *Nature* **2003**, *424* (6952), 1057–61.

(14) Cao, Z. B.; Chen, X.; Yao, J. R.; Huang, L.; Shao, Z. Z. The preparation of regenerated silk fibroin microspheres. *Soft Matter* **2007**, *3* (7), 910–915.

(15) Zhang, F.; You, X.; Dou, H.; Liu, Z.; Zuo, B.; Zhang, X. Facile Fabrication of Robust Silk Nanofibril Films via Direct Dissolution of Silk in CaCl2–Formic Acid Solution. *ACS Appl. Mater. Interfaces* **2015**, *7* (5), 3352–3361.

(16) Pereira, R. F. P.; Sentanin, F.; Pawlicka, A.; Goncalves, M. C.; Silva, M. M.; Bermudez, V. D. Smart Windows Prepared from Bombyx mori Silk. *ChemElectroChem* **2016**, *3* (7), 1084–1097.

(17) Lu, S.; Wang, P.; Zhang, F.; Zhou, X.; Zuo, B.; You, X.; Gao, Y.; Liu, H.; Tang, H. A novel silk fibroin nanofibrous membrane for guided bone regeneration: a study in rat calvarial defects. *Am. J. Transl. Res.* **2015**, *7*, 2244–53.

(18) Liu, Q.; Wang, F.; Gu, Z.; Ma, Q.; Hu, X. Exploring the Structural Transformation Mechanism of Chinese and Thailand Silk Fibroin Fibers and Formic-Acid Fabricated Silk Films. *Int. J. Mol. Sci.* **2018**, *19* (11), 3309.

DOI: 10.1021/acsbiomaterials.9b00577
ACS Biomater. Sci. Eng. 2019, 5, 6361–6373

(19) Wang, F.; Yu, H. Y.; Gu, Z. G.; Si, L.; Liu, Q. C.; Hu, X. Impact of calcium chloride concentration on structure and thermal property of Thai silk fibroin films. *J. Therm. Anal. Calorim.* **2017**, *130* (2), 851−859.
(20) Yue, X.; Zhang, F.; Wu, H.; Ming, J.; Fan, Z.; Zuo, B. J. M. L. A novel route to prepare dry-spun silk fibers from CaCl2−formic acid solution. *Mater. Lett.* **2014**, *128*, 175−178.
(21) Zhang, F.; Lu, Q.; Yue, X.; Zuo, B.; Qin, M.; Li, F.; Kaplan, D. L.; Zhang, X. J. A. b. Regeneration of high-quality silk fibroin fiber by wet spinning from CaCl2−formic acid solvent. *Acta Biomater.* **2015**, *12*, 139−145.
(22) Yang, R.; Wu, P.; Wang, X.; Liu, Z.; Zhang, C.; Shi, Y.; Zhang, F.; Zuo, B. J. R. a. A novel method to prepare tussah/Bombyx mori silk fibroin-based films. *RSC Adv.* **2018**, *8* (39), 22069−22077.
(23) Liu, Q.; Wang, F.; Gu, Z.; Ma, Q.; Hu, X. J. I. j. o. m. s. Exploring the structural transformation mechanism of chinese and Thailand silk fibroin fibers and formic-acid fabricated silk films. *Int. J. Mol. Sci.* **2018**, *19* (11), 3309.
(24) Tao, H.; Kaplan, D. L.; Omenetto, F. G. Silk materials−a road to sustainable high technology. *Adv. Mater.* **2012**, *24* (21), 2824−2837.
(25) Rockwood, D. N.; Preda, R. C.; Yucel, T.; Wang, X.; Lovett, M. L.; Kaplan, D. L. Materials fabrication from Bombyx mori silk fibroin. *Nat. Protoc.* **2011**, *6* (10), 1612−31.
(26) Leal-Egaña, A.; Scheibel, T. Silk-based materials for biomedical applications. *Biotechnol. Appl. Biochem.* **2010**, *55* (3), 155−167.
(27) Lammel, A. S.; Hu, X.; Park, S. H.; Kaplan, D. L.; Scheibel, T. R. Controlling silk fibroin particle features for drug delivery. *Biomaterials* **2010**, *31* (16), 4583−91.
(28) Jao, D.; Xue, Y.; Medina, J.; Hu, X. Protein-Based Drug-Delivery Materials. *Materials* **2017**, *10* (5), 517.
(29) Wang, F.; Wolf, N.; Rocks, E. M.; Vuong, T.; Hu, X. Comparative studies of regenerated water-based Mori, Thai, Eri, Muga and Tussah silk fibroin films. *J. Therm. Anal. Calorim.* **2015**, *122* (3), 1069−1076.
(30) Xue, Y.; Jao, D.; Hu, W. B.; Hu, X. Silk-silk blend materials. *J. Therm. Anal. Calorim.* **2017**, *127* (1), 915−921.
(31) Hu, X.; Kaplan, D.; Cebe, P. Determining beta-sheet crystallinity in fibrous proteins by thermal analysis and infrared spectroscopy. *Macromolecules* **2006**, *39* (18), 6161−6170.
(32) Hu, X.; Lu, Q.; Kaplan, D. L.; Cebe, P. Microphase separation controlled β-sheet crystallization kinetics in fibrous proteins. *Macromolecules* **2009**, *42* (6), 2079−2087.
(33) Mazzi, S.; Zulker, E.; Buchicchio, J.; Anderson, B.; Hu, X. Comparative thermal analysis of Eri, Mori, Muga, and Tussar silk cocoons and fibroin fibers. *J. Therm. Anal. Calorim.* **2014**, *116* (3), 1337−1343.
(34) Lu, Q.; Wang, X.; Hu, X.; Cebe, P.; Omenetto, F.; Kaplan, D. L. Stabilization and release of enzymes from silk films. *Macromol. Biosci.* **2010**, *10* (4), 359−68.
(35) Hu, X.; Lu, Q.; Sun, L.; Cebe, P.; Wang, X.; Zhang, X.; Kaplan, D. L. Biomaterials from ultrasonication-induced silk fibroin-hyaluronic acid hydrogels. *Biomacromolecules* **2010**, *11* (11), 3178−88.
(36) Zhang, J.; Rajkhowa, R.; Li, J. L.; Liu, X. Y.; Wang, X. G. Silkworm cocoon as natural material and structure for thermal insulation. *Mater. Eng.* **2013**, *49*, 842−849.
(37) Goormaghtigh, E.; Cabiaux, V.; Ruysschaert, J. M. Secondary structure and dosage of soluble and membrane proteins by attenuated total reflection Fourier-transform infrared spectroscopy on hydrated films. *Eur. J. Biochem.* **1990**, *193* (2), 409−20.
(38) Dong, A.; Huang, P.; Caughey, W. S. Protein secondary structures in water from second-derivative amide I infrared spectra. *Biochemistry* **1990**, *29* (13), 3303−8.
(39) Mouro, C.; Jung, C.; Bondon, A.; Simonneaux, G. Comparative Fourier transform infrared studies of the secondary structure and the CO heme ligand environment in cytochrome P-450cam and cytochrome P-420cam. *Biochemistry* **1997**, *36* (26), 8125−34.
(40) Tretinnikov, O. N.; Tamada, Y. Influence of casting temperature on the near-surface structure and wettability of cast silk fibroin films. *Langmuir* **2001**, *17* (23), 7406−7413.
(41) Teramoto, H.; Miyazawa, M. Molecular orientation behavior of silk sericin film as revealed by ATR infrared spectroscopy. *Biomacromolecules* **2005**, *6* (4), 2049−57.
(42) Schneider, J. P.; Pochan, D. J.; Ozbas, B.; Rajagopal, K.; Pakstis, L.; Kretsinger, J. Responsive hydrogels from the intramolecular folding and self-assembly of a designed peptide. *J. Am. Chem. Soc.* **2002**, *124* (50), 15030−7.
(43) Pochan, D. J.; Schneider, J. P.; Kretsinger, J.; Ozbas, B.; Rajagopal, K.; Haines, L. Thermally reversible hydrogels via intramolecular folding and consequent self-assembly of a de novo designed peptide. *J. Am. Chem. Soc.* **2003**, *125* (39), 11802−3.
(44) Chen, X.; Shao, Z.; Knight, D. P.; Vollrath, F. Conformation transition kinetics of Bombyx mori silk protein. *Proteins: Struct., Funct., Genet.* **2007**, *68* (1), 223−31.
(45) Du, N.; Yang, Z.; Liu, X. Y.; Li, Y.; Xu, H. Y. Structural origin of the strain-hardening of spider silk. *Adv. Funct. Mater.* **2011**, *21* (4), 772−778.
(46) Kinahan, M. E.; Filippidi, E.; Koster, S.; Hu, X.; Evans, H. M.; Pfohl, T.; Kaplan, D. L.; Wong, J. Tunable Silk: Using Microfluidics to Fabricate Silk Fibers with Controllable Properties. *Biomacromolecules* **2011**, *12* (5), 1504−1511.
(47) Wang, H. Y.; Zhang, Y. Q. Effect of regeneration of liquid silk fibroin on its structure and characterization. *Soft Matter* **2013**, *9* (1), 138−145.
(48) Lu, S.; Li, J.; Zhang, S.; Yin, Z.; Xing, T.; Kaplan, D. L. The influence of the hydrophilic−lipophilic environment on the structure of silk fibroin protein. *J. Mater. Chem. B* **2015**, *3* (13), 2599−2606.
(49) Hu, X.; Kaplan, D.; Cebe, P. Dynamic protein- water relationships during β-sheet formation. *Macromolecules* **2008**, *41* (11), 3939−3948.
(50) Hu, X.; Shmelev, K.; Sun, L.; Gil, E. S.; Park, S. H.; Cebe, P.; Kaplan, D. L. Regulation of silk material structure by temperature-controlled water vapor annealing. *Biomacromolecules* **2011**, *12* (5), 1686−96.
(51) Jin, H. J.; Park, J.; Karageorgiou, V.; Kim, U. J.; Valluzzi, R.; Cebe, P.; Kaplan, D. L. Water-Stable Silk Films with Reduced β-Sheet Content. *Adv. Funct. Mater.* **2005**, *15* (8), 1241−1247.
(52) Fu, C.; Porter, D.; Chen, X.; Vollrath, F.; Shao, Z. Understanding the mechanical properties of Antheraea pernyi silk—from primary structure to condensed structure of the protein. *Adv. Funct. Mater.* **2011**, *21* (4), 729−737.
(53) Andiappan, M.; Sundaramoorthy, S.; Panda, N.; Meiyazhaban, G.; Winfred, S. B.; Venkataraman, G.; Krishna, P. Electrospun eri silk fibroin scaffold coated with hydroxyapatite for bone tissue engineering applications. *Prog. Biomater* **2013**, *2* (1), 6.
(54) Li, M. Z.; Tao, W.; Kuga, S.; Nishiyama, Y. Controlling molecular conformation of regenerated wild silk fibroin by aqueous ethanol treatment. *Polym. Adv. Technol.* **2003**, *14* (10), 694−698.
(55) Li, M.; Tao, W.; Kuga, S.; Nishiyama, Y. J. P. f. A. T. Controlling molecular conformation of regenerated wild silk fibroin by aqueous ethanol treatment. *Polym. Adv. Technol.* **2003**, *14* (10), 694−698.
(56) Ling, S.; Qin, Z.; Li, C.; Huang, W.; Kaplan, D. L.; Buehler, M. J. Polymorphic regenerated silk fibers assembled through bioinspired spinning. *Nat. Commun.* **2017**, *8* (1), 1387.
(57) Hu, X.; Kaplan, D.; Cebe, P. Effect of water on the thermal properties of silk fibroin. *Thermochim. Acta* **2007**, *461* (1−2), 137−144.
(58) Wunderlich, B.; Jin, Y. M.; Boller, A. Mathematical-Description of Differential Scanning Calorimetry Based on Periodic Temperature Modulation. *Thermochim. Acta* **1994**, *238*, 277−293.
(59) Cebe, P.; Hu, X.; Kaplan, D. L.; Zhuravlev, E.; Wurm, A.; Arbeiter, D.; Schick, C. Beating the Heat - Fast Scanning Melts Silk Beta Sheet Crystals. *Sci. Rep.* **2013**, *3*, 1 DOI: 10.1038/srep01130.

DOI: 10.1021/acsbiomaterials.9b00577
ACS Biomater. Sci. Eng. 2019, 5, 6361−6373

(60) Wang, X.; Yucel, T.; Lu, Q.; Hu, X.; Kaplan, D. L. Silk nanospheres and microspheres from silk/pva blend films for drug delivery. *Biomaterials* **2010**, *31* (6), 1025−35.
(61) Wang, X.; Kluge, J. A.; Leisk, G. G.; Kaplan, D. L. Sonication-induced gelation of silk fibroin for cell encapsulation. *Biomaterials* **2008**, *29* (8), 1054−64.
(62) Park, S. H.; Gil, E. S.; Shi, H.; Kim, H. J.; Lee, K.; Kaplan, D. L. Relationships between degradability of silk scaffolds and osteogenesis. *Biomaterials* **2010**, *31* (24), 6162−6172.
(63) Hu, X.; Wang, X.; Rnjak, J.; Weiss, A. S.; Kaplan, D. Biomaterials derived from silk−tropoelastin protein systems. *Biomaterials* **2010**, *31* (32), 8121−8131.
(64) Hu, X.; Park, S. H.; Gil, E. S.; Xia, X. X.; Weiss, A. S.; Kaplan, D. L. The influence of elasticity and surface roughness on myogenic and osteogenic-differentiation of cells on silk-elastin biomaterials. *Biomaterials* **2011**, *32* (34), 8979−89.
(65) Lu, Q.; Hu, X.; Wang, X.; Kluge, J. A.; Lu, S.; Cebe, P.; Kaplan, D. L. Water-insoluble silk films with silk I structure. *Acta Biomater.* **2010**, *6* (4), 1380−7.
(66) Bai, S.; Liu, S.; Zhang, C.; Xu, W.; Lu, Q.; Han, H.; Kaplan, D. L.; Zhu, H. Controllable transition of silk fibroin nanostructures: An insight into in vitro silk self-assembly process. *Acta Biomater.* **2013**, *9* (8), 7806−7813.
(67) Callone, E.; Dire, S.; Hu, X.; Motta, A. Processing Influence on Molecular Assembling and Structural Conformations in Silk Fibroin: Elucidation by Solid-State NMR. *ACS Biomater. Sci. Eng.* **2016**, *2* (5), 758−767.
(68) Inoue, S.-i.; Tsuda, H.; Tanaka, T.; Kobayashi, M.; Magoshi, Y.; Magoshi, J. Nanostructure of Natural Fibrous Protein: In Vitro Nanofabric Formation of Samia c ynthia r icini Wild Silk Fibroin by Self-Assembling. *Nano Lett.* **2003**, *3* (10), 1329−1332.
(69) Zhou, P.; Xie, X.; Knight, D. P.; Zong, X.-H.; Deng, F.; Yao, W.-H. Effects of pH and calcium ions on the conformational transitions in silk fibroin using 2D Raman correlation spectroscopy and 13C solid-state NMR. *Biochemistry* **2004**, *43* (35), 11302−11311.

DOI: 10.1021/acsbiomaterials.9b00577
ACS Biomater. Sci. Eng. 2019, 5, 6361−6373